Materials & Design 251 (2025) 113578

Contents lists available at ScienceDirect

Materials & Design

journal homepage: www.elsevier.com/locate/matdes

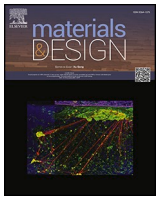

Impact of accelerated corrosion on weld geometry, hardness and residual stresses of offshore steel joints over time

Sulaiman Shojai [a,b,*], Finn Schönamsgruber [a], Markus Köhler [c], Elyas Ghafoori [a]

[a] Leibniz University Hannover, Institute for Steel Construction ForWind, Hannover, Germany
[b] German Aerospace Center (DLR), Institute of Maritime Energy Systems, Geesthacht, Germany
[c] Institute of Joining and Welding, Technische Universität Braunschweig, Braunschweig, Germany

ARTICLE INFO

Keywords:
Offshore-wind
Digital scans
Corrosion fatigue
Stress concentrations
Welds
Residual stress
Hardness

ABSTRACT

Corrosion of offshore support structures can reduce the estimated fatigue life. Pitting corrosion, in particular, is known to lead to local stress concentrations and thus reduce their service life. However, offshore support structures consist of a large number of weld seams, which already have their own stress concentrations and interact with pitting corrosion. So far, there have been no studies on how corrosion can influence the stress concentrations on a long-term basis. In this study, butt- and fillet-welded specimens were exposed to corrosion in a salt spray chamber for up to 12 months and their geometrical development was examined using 3D scans. In addition, hardness and residual stress measurements were carried out. The results were compared to specimens, which were corroded for 12 months in artificial seawater. It could be shown that corrosion causes the notches of the butt welds to become sharper over time, while the fillet welds become narrower. It could be also shown that despite existing scatter, the residual stresses do not change significantly over time. The hardness measurements revealed that although there are no significant changes in the hardness values, the location of the sharpest notch shifted repeatedly within the weld metal, heat affected zone, and base material, which had different hardness values.

1. Introduction

Offshore support structures are exposed to harsh environmental conditions and fatigue loads. In such conditions, the corrosion protection system has a limited service life. In case the protection system is deteriorated or damaged, free corrosion may occur. Pitting corrosion, in particular, act as geometrical notches, which may lead to strong local stress concentrations and reduce the fatigue strength of the support structures and thus the (remaining) service life.

The influence of pitting corrosion on the stress concentrations of steel plates has already been investigated in many studies, such as [1–3] with main focus on single pit and [4–6] on multiple pit geometry. In reality, however, steel structures consist of a large number of welded joints that already include stress concentrations from the weld seam geometry. The relationship between the weld seam geometry in the uncorroded state and their fatigue strength has already been demonstrated and proven in many studies [7–11].

Regarding the geometrical influence of weld seams on the fatigue properties, the weld geometry can be characterized by two important parameters: the weld toe radius r and the flank angle θ as per ISO 5817 standards [12]. The stress concentration factor (SCF), also notch factor K_t, can be derived from these geometrical parameters based on analytical formulations of different authors such as Lawrence et al. [13], Anthes et al. [14] or Kiyak et al. [15].

However, the investigations on weld geometry are limited to the uncorroded state. Only a few reports, such as those by Matsushita et al. [16] and Yuasa and Watanabe [17], which were summarized by Jakubowski [18], deal with the geometrical change of weld seams under corrosive influence. Matsushita et al. [16] evaluated pre-corroded fillet-welded joints of different exposure duration, which were taken from a former tanker and found, that more material was removed in the area of the weld toe, which corresponds with the heat affected zone (HAZ), than in other areas of fillet-welded joints. The local removal led to a groove in the area and is referred to as grooving corrosion. Yuasa and Watanabe [17] exposed fillet- and butt-welded specimens to corrosion for three and six months and could observe similar behaviour of grooving development at the weld toe for mild steel. Subsequent fatigue tests on the pre-corroded specimens showed that the fatigue strength of the butt-

* Corresponding author.
E-mail address: sulaiman.shojai@dlr.de (S. Shojai).

https://doi.org/10.1016/j.matdes.2024.113578
Received 16 July 2024; Received in revised form 9 December 2024; Accepted 27 December 2024
Available online 6 January 2025

welded joints decreased, while it remained the same for the fillet-welded joints. It was argued that the already very sharp notches of the fillet welds could not be further intensified by corrosion, while the butt welds had more potential of being sharpened due to the low initial notch sharpness. However, there was no comprehensive examination of the change in the weld geometry due to the corrosive effect at that time.

The corrosion test in the investigation of Yuasa and Watanabe [17] included repeated wet and dry periods of 6 h in the laboratory. Other corrosion test methods in the laboratory are immersion test in artificial seawater (ASW) according to ASTM D1141 [19] or the salt spray chamber (SSC) test according to ISO 9277 [20]. Corrosion in ASW predominantly causes uniform corrosion and cannot replicate the irregular surface typically observed at the splash zone, while the SSC test leads to more irregular corrosion. This observation was confirmed by Gkatzogiannis et al. [21] in which the correlation of laboratory and real marine corrosion behavior was investigated. Additionally, it was shown that the roughness correlated with fatigue strength and that the mean roughness after one year in real corrosion environment (here: splash zone of offshore support structures) corresponded to that of corroded specimens exposed to corrosion for 20 days in the SSC. This results in an acceleration ratio of approx. 18, while the same study only gives an acceleration ratio of 3.5 for thickness loss. Although the SSC method cannot reproduce the development of corrosion to the full extent, the SSC method is a preferred test method due to its ability to replicate irregular surfaces of the splash zone.

The first quantitative study on the influence of corrosion on the geometrical parameters of weld seams based on 2D scans was presented by Weinert et al. [22] for 10-day SSC and 30-day ASW exposures. In [23] the authors of this paper investigated specimens using 3D-scans, which were stored in SSC for a period of one month. Compared to the total lifetime of offshore support structures of at least 20 years, these exposure durations can be considered as short-term. In order to quantify the long-term behavior, however, longer exposure durations need to be investigated.

In addition to the weld seam geometry, other parameters such as the local material properties or residual stresses [24–29] play a major role in fatigue. High local material strengths, which correlate with high hardness values, lead to lower plastic strains and therefore to less damage under fatigue loading. At the same time, high residual tensile stresses may lead to early crack initiation and a shorter overall fatigue life. It has been shown that consideration of these parameters can achieve a reduction in the scatter of fatigue tests [30–33] and thus contribute to greater reliability of fatigue assessment. Analogous to the geometrical parameters, there is also a knowledge gap in local material behaviour and residual stresses with regard to long-term corrosive effects.

In order to close this gap, butt- and fillet-welded specimens are stored in a SSC for a total of 12 months for accelerated corrosion exposure and specimens are taken successively every three months. These specimens are examined and statistically analysed for geometrical changes in the weld seams using 3D-scans before and after the corrosion process. In addition, residual stress measurements and hardness measurements are carried out on the specimens in order to analyse the development over time. Finally, the results were qualitatively compared with specimens corroded for 12 months in ASW.

The novelties of this study can be summarized as follows:

- Investigation of weld geometry changes due to corrosion based on digital scans
- Probabilistic evaluation of stress concentrations based on weld geometry
- Change in hardness and residual stress due to corrosion
- Variations in the above parameters over time

These parameters are essential in order to predict the (remaining) service life of corroded steel structures with sufficient accuracy and to make fundamental decisions about possible repair or replacement measures.

2. Experiments

2.1. Specimen preparation and corrosion exposure

2.1.1. Specimen preparation

In the framework of this study, welded specimens made of low-alloy structural steel S355 ML were investigated. For the welded specimens, double V-shaped butt welds (S) and fillet welds (K) were examined. Specimens with fillet welds included non-load carrying transverse stiffeners, which were welded on a continuous plate with a throat thickness of 4 mm. Fillet welds were produced using the gas metal arc welding (GMAW) process, with filler material EN ISO 17632-A: T46 6 M M 1 H5, and the butt welds using the submerged arc welding (SAW) process, with filler material EN ISO 14171-A: S3Si. In both cases, the limits for irregularities were in line with the evaluation group B according to ISO 5817 [12]. The specimen geometries are shown in Fig. 1. After welding, the specimens were cut by water jet. Then, the specimens were clean blasted analogues to real offshore support structures. For the investigated specimens, cleanliness grades of Sa 2 ½ to 3 according to ISO 8501–1 [34] and DNV RP-0416 [35] were achieved.

2.1.2. Corrosion exposure

After preparation, the specimens were stored in the standardized neutral SSC test with a 5 % natrium-chloride solution according to ISO 9227 [20] in order to accelerate the corrosion process. Therefore, the steel specimens were placed at an angle between 15° and 20° from the vertical so that the surfaces were fully exposed to the salt spray. For more details on the SSC test it is referred to [23]. The specimens were stored in the SSC for up to 12 months. Specimens were successively taken from the SSC after 3, 6 and 9 months of storage. To compare the accelerated corrosion in the SSC with more realistic conditions, specimens were also stored in ASW in accordance with ASTM D1141 [19] for 12 months. A total of 19 specimens, which are summarized in a test matrix in Table 1, were examined with regard to their corrosion behaviour. In the matrix shown, a distinction is made between the specimen geometry and the type and duration of corrosion exposure. The first digit of the specimen's notation refers to the corrosion exposure time, the second to the geometry, and the third to the specimen's number, while with (S) the exposure in ASW is denoted.

The rust on the specimens was removed according ISO 8407–1 [36] including mechanical treatment with a wire brush and a subsequent

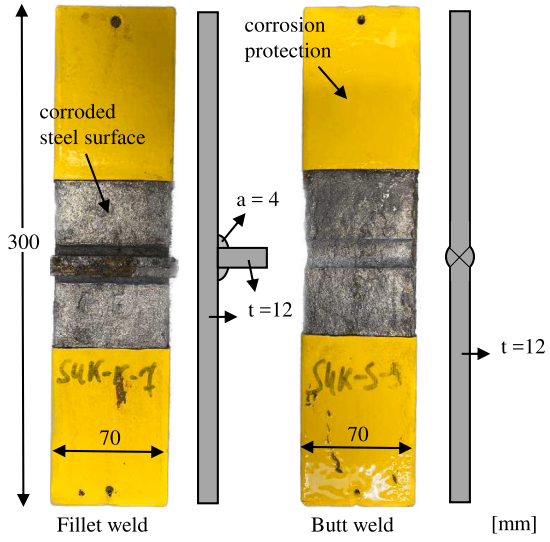

Fig. 1. Specimen geometries and corroded surface after rust removal for fillet- and butt-welded specimens.

Table 1
Test matrix including different surface conditions and weld types.

Specimen No.	Geometry		Corrosion exposure	
	Butt weld	Fillet welds	Corroded in neutral salt spray chamber (SSC)	Corroded in artificial seawater (ASW)
3-S-6	x		3 months	
3-S-7	x		3 months	
6-S-8	x		6 months	
9-S-9	x		9 months	
12-S-11	x		12 months	
12-S-1 (S)	x			12 months
3-K-1		x	3 months	
3-K-2		x	3 months	
3-K-3		x	3 months	
6-K-4		x	6 months	
6-K-5		x	6 months	
6-K-6		x	6 months	
9-K-7		x	9 months	
9-K-8		x	9 months	
9-K-9		x	9 months	
12-K-5		x	12 months	
12-K-6		x	12 months	
12-K-8		x	12 months	
12-K-1 (S)		x		12 months

hydrochloric acid bath for around 5–20 min, which was prepared in the ratio of 1000 ml hydrochloric acid (HCl), 20 g antimony trioxide (Sb_2O_3) and 50 g tin(II)chloride ($SnCl_2$). In Fig. 1, the specimen geometries after 9 months corrosion exposure in SSC are illustrated after rust removal.

2.2. 3D-scans

The scans were performed using the GOM ATOS Core 300 optical 3D scanner with a resolution of 0.12 mm. The scanner was placed at a distance of 50 cm from the specimen on a rotatable plate in order to capture images from different angles, see Fig. 2 (a). The scans were automatically merged using the GOM Suite software, requiring sufficient reference points in each scan. Therefore, multiple reference points were placed on the rotatable plate. Four scans per side were found to be adequate for comprehensive coverage of the specimen. Additional reference points were positioned on the sides of the specimen to merge both sides of the specimen into one model, as shown in Fig. 2 (c) and (d). The reference points resulted in holes in the model, which were filled with the GOM Suite software during post-processing, as illustrated in Fig. 2 (b).

This scanning process was carried out for all specimens listed in Table 1. The specimens were scanned directly after welding in the as-welded (AW) condition, after the subsequent clean blasting (CB) and after corrosion exposure, denoted as e.g. 3 M or 9 M, where the number corresponds to the exposure duration in months. The result of the scanning process was a STL file, representing a closed surface generated from a point cloud via triangulation. The subsequent digital comparison of the models was conducted within the GOM Suite software. Both models were imported into a single project and aligned manually. After alignment, the scans were overlaid using the best-fit command of the software, which is based on the least square approximation method. To achieve accurate comparisons, it was crucial for the specimens to share as many surface areas as possible. This was ensured by the area of corrosion protection, which remained the same after corrosion exposure.

However, it should be noted that because of the low resolution of ATOS Core 300 scanner, the scans were only used for a qualitative comparison before and after corrosion. For the following quantitative analysis of the weld geometry parameters, the specimens were additionally scanned with the Keyence VR 3000 profilometer, with a resolution of approx. 0.02 mm.

2.3. Geometrical weld parameters and stress concentration factors

The weld geometry of steel components plays a crucial role in fatigue analysis, as it directly influences the fatigue defining stress concentra-

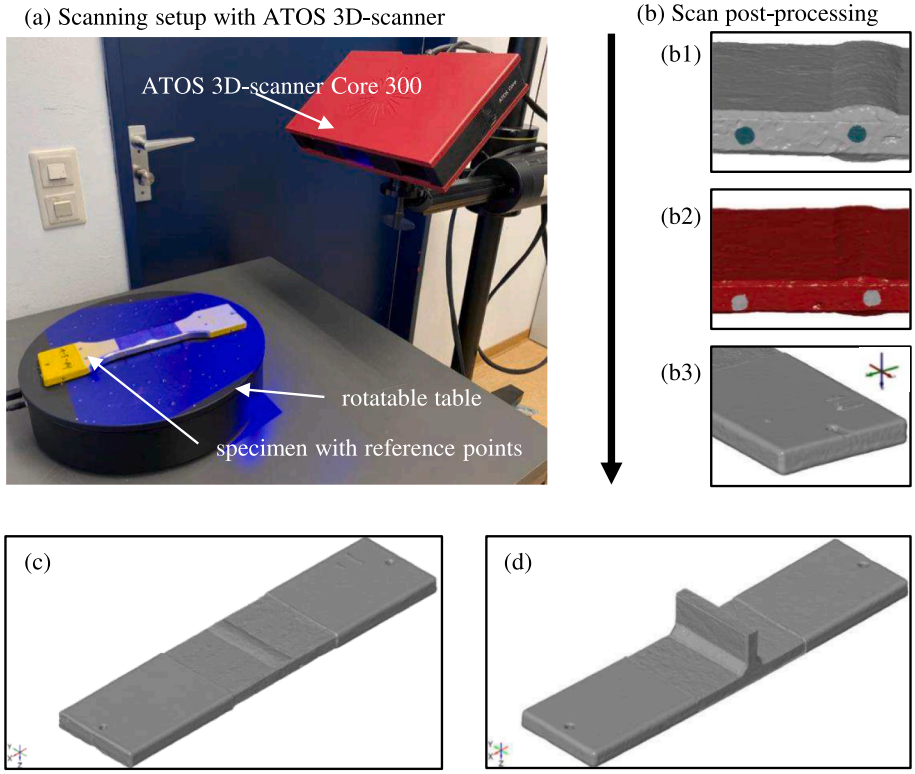

Fig. 2. Digital 3D-scans using ATOS Core 300: (a) test setup, (b) scan post-processing (c) scan of butt-welded specimen and (d) scan of fillet-welded specimen.

tions. The weld geometry can be characterized mainly by weld toe radius r and the flank angle θ, see Fig. 3 (a). There are different analytical formulations, as stated in the introduction, in order to calculate the stress concentration factor (SCF), also referred to as notch factor K_t. Alternatively, it is possible to include the real geometrical parameter in numerical analysis in combination of one of many theories for micro-support consideration such as the theory of critical distance [37]. Since the focus of this work was more on the development of the geometrical parameter over time, the equation (1) proposed by Anthes et al. [14] was used to analyse the SCF for the sake of simplicity.

$$SCF = K_t = 1 + 0.728(sin(180^\circ - \theta))^{0.932}\left(\frac{t}{r}\right)^{0.382} \quad (1)$$

Here, the SCF depends on the weld toe radius (r), the flank angle (θ), which can also be interpreted as an opening angle, and the component thickness (t). It tends to increase with larger flank angles, greater notch radii, and smaller thicknesses. Understanding the impact of corrosion on fatigue necessitates an analysis of these geometrical parameters and their changes due to corrosion exposure.

The weld seam geometry can be evaluated automatically based on algorithms proposed Renken et al. [38], Schubnell [39], Dänekas et al. [40,41], and Heide et al. [42]. In this study, the weld geometry was quantified using a MATLAB tool presented in Shojai et al. [23], which was developed especially for corroded weld seams. For the evaluation, the scans were exported in ASCII file format and were therefore available as a point cloud. No points were skipped during export; hence the distance between each point was approx. 0.02 mm, according to the resolution. The weld geometry parameters were evaluated based on cross sections in the longitudinal direction, see Fig. 3 (b), which was performed by the MATLAB tool. The distance between each cross-section line was 0.02 mm, consistent to the resolution. For each cross-section line, the first and second derivatives were calculated in the first step. The first derivative was used to find the point minimum slope in the section line, which corresponds with the notch toe at point B according to Fig. 3 (c) and the second derivative was used to derive the maximum slope in the section line, which corresponds to point A in in Fig. 3 (c). Point B was used to create two balance lines: from point B in the direction of the base material, and from point B to point A. The angle between those two balance lines corresponds to the flank angle. The intersection of these two lines serves as the starting point for the circle, which is placed in the notch toe as an approximation for the weld toe radius. The radius of the circle was determined by fitting the circle into the real data of the cross-section line based on the minimum sum of squared deviations.

The weld parameters were determined for the butt and fillet weld samples in all three surface condition (AW, CB and corroded). The butt-welded specimens contained four weld toes per specimen, for the fillet-welded specimens only two welds were considered.

It should be noted that the presented tool uses the local minimum and the highest slope corresponding to point A and B, in order to derive the weld geometry. In the process of corrosion development, large pits are sometimes formed that are located outside the weld seam but match the criteria for points A and B mentioned above. In order to avoid incorrect results arising from this, the tool examines the locations at which the parameters were determined and checks whether these are consistent with the locations on the other cross-section lines. If they do not match, the results are not taken into account. This led to a different number of examined cross-sections for the specimens with the same width.

2.4. Hardness and residual stress measurements

2.4.1. Hardness measurement

For hardness assessment, cross-sections of the welded joints were examined using a QNess Q10A + device. This facilitated automated hardness mapping by integrating both the indenter and the measuring microscope. Vickers hardness was measured in accordance with ISO 6507–1 standards [43]. Given that the effects of corrosion are most pronounced near the surface, hardness measurements were performed with a testing load according to HV 0.1, in order to enable near surface measurements. Using HV 0.1, hardness could be determined up to a distance of 75 µm from the surface, with a spacing of 100 µm between indentations.

2.4.2. Residual stress measurements

Residual stress was assessed on the surface of the specimens using X-ray diffraction (XRD) employing the sin2ψ technique with copper radiation. Diffraction patterns were obtained at 11 angles between $\Psi = 159^\circ$ and 161°, utilizing a collimator diameter of 2 mm. This setup yielded a measurement spot of approximately 2.0–2.5 mm in diameter, with diffraction information averaged over the spot. The depth of the diffraction information was approximately 5 µm. Measurements were conducted along a measuring path perpendicular to the weld seam, commencing at the weld toe. To accurately represent the anticipated stress gradients, the distances between individual measuring points were kept smaller than the spot diameter. At each measuring point, stress components in both longitudinal and transverse direction in relation to the weld path were measured, with transverse stress components aligned with the specimen's loading direction.

3. Experimental results and discussion

3.1. 3D-scan results

3.1.1. Salt spray chamber specimens

The intention of the digital surface comparison is to make qualitative statements about the corrosion development over time. For this purpose, the relatively low resolution of the ATOS Core System of 0.12 mm is assumed to be sufficient.

The results of the digital surface comparisons are shown in Fig. 4 and Fig. 5 for increasing corrosion exposure duration from three months shown in subplots (a) to 12 months on the right (d). In subplots (a1) to

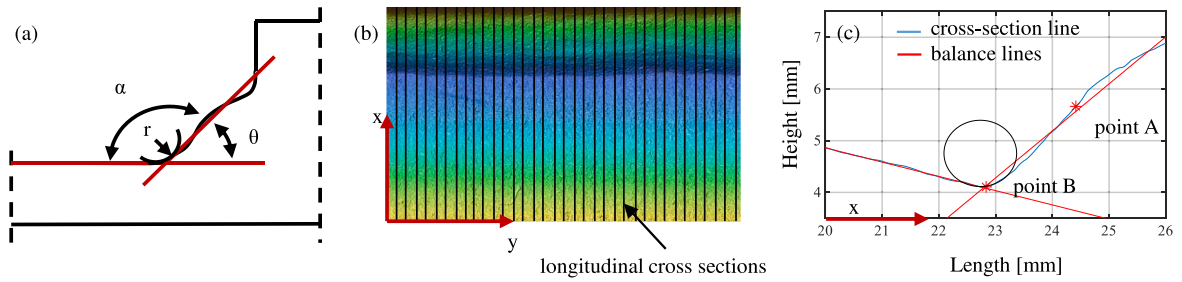

Fig. 3. (a) Geometrical weld parameters according ISO 5817 [12], (b) longitudinal cross sections through weld seam, and (c) evaluation of geometrical parameters in the MATLAB tool.

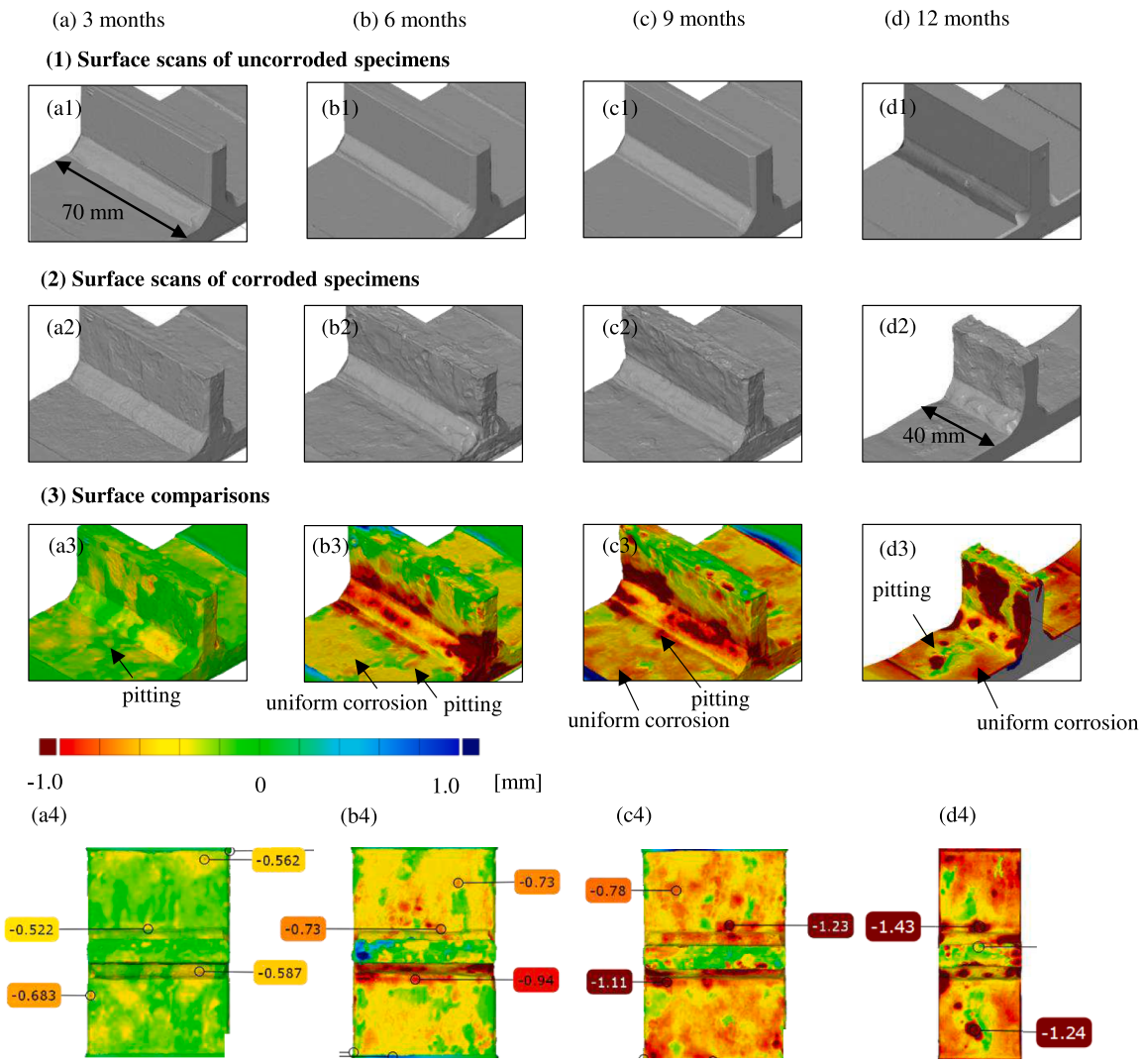

Fig. 4. Results of surface scans for fillet welds, (a1-d1) scans in uncorroded condition, (a2-d2) scan after corrosion exposure, (a3-d3) deviation plot of the scans, (a4-d4) deviation plot with deviation banners.

(d1) the scans of the CB condition and in (a2) to (d2) the scans of the corroded condition are illustrated. Subplots (a3) to (d3) depict the deviation between the scans before and after corrosion exposure. Subplots (a4) to (d4) show specific values of the material removal at some selected points with deviation flags in [mm].

As a general trend, it can be observed that material removal increases with increasing corrosion duration. This can be noticed by the increase of red areas. On the base material, a combination of uniform and localized pitting corrosion can be seen. For example, extensive uniform corrosion can be seen on the base material of the fillet-welded specimens on Fig. 4 (b3), (c3) and (d3) as well as on the butt-welded specimen in Fig. 5 (b3), (c3) and (d) after six, nine and 12 months of corrosion exposure. On the other hand, pitting corrosion on the base material can be seen in every plot of Fig. 4 and Fig. 5. In contrast to the total material removal, which increases over the corrosion duration, no steady increase can be observed in the pitting depths. While the increase in pitting depths between three and six months of exposure is significant, compare e.g. attached stiffener in Fig. 4 (a3) and (b3), the increase between six and nine months is very low. After 12 months, the pit depths are partially lower (see attached stiffener in Fig. 4 (d3)) than after nine months, which can be attributed to the merging of individual pits. This is consistent with the observations of Melchers [44], in which individual pits initially grow in plate thickness and then spread in lateral direction by merging and forming a new plateau. The initial pitting corrosion tends to become uniform corrosion over time, whereby the process can be repeated on the new plateau and can therefore be described as a cyclic behaviour of corrosion development.

Furthermore, it can be observed that pitting corrosion develops directly on the weld toe, which already has strong stress concentrations due to the weld seam geometry, see Fig. 4 (b3) and (c3) and Fig. 5 (b3), (c3) and (d3). Moreover, it can be observed that, in addition to individual pronounced pits, a groove forms on the weld toe over the entire length of the weld seam, see e.g. Fig. 4 (b3) or Fig. 5 (b3). This can be observed especially from an exposure duration of six months and is referred to in the literature as grooving corrosion [16,18]. Accordingly, the main reason for this is the electrochemical potential, as the material at the weld toe, which lies entirely in the heat affected zone (HAZ), is less noble than the base material due to different phase composition and lattice imperfections. Moreover, the finer grain structures, inclusions, and phase boundaries in the HAZ, act as preferred sites for pit initiation. These differences are not due to composition but arise from localized microstructural characteristics [45,46].

Increased material removal due to unequal water deposition in the corrosion test can be ruled out due to the inclined storage of the specimens in the test.

The comparison between fillet-welded and butt-welded joints, e.g. Fig. 4 (b3) or Fig. 5 (b3), also shows that grooving corrosion is more pronounced on fillet welds than on butt welds, while pitting corrosion is

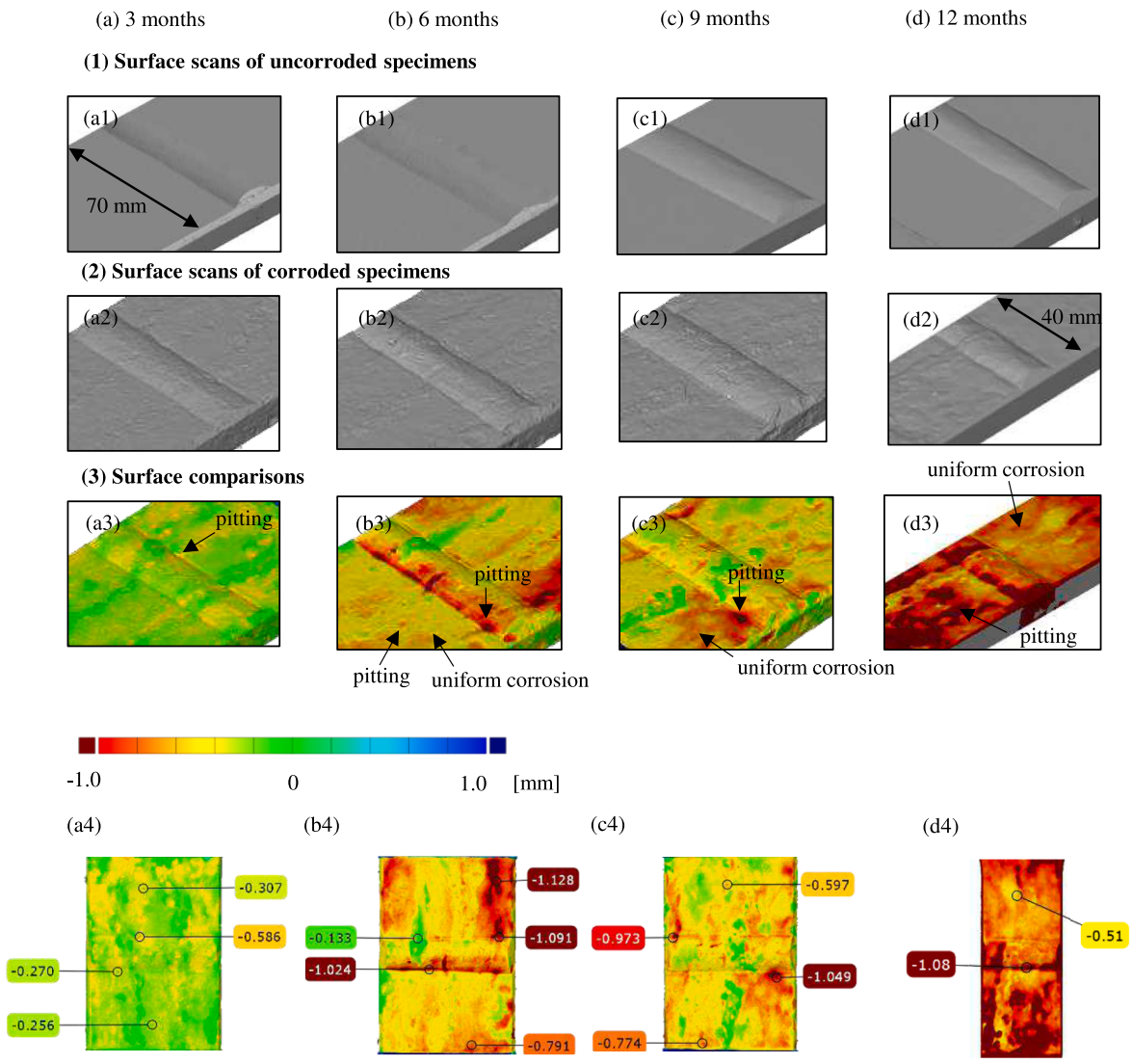

Fig. 5. Results of surface scans for butt welds, (a1-d1) scans in uncorroded condition, (a2-d2) scan after corrosion exposure, (a3-d3) deviation plot of the scans, (a4-d4) deviation plot with deviation banners.

more pronounced on butt welds than on fillet welds. For the fillet-welded specimens, it can be observed that after six months of exposure the grooving corrosion is pronounced over a broad width, while on butt-welded specimen it is more localized directly in the weld toe. Despite the partially different characteristics of grooving corrosion between fillet and butt welds, a cyclical behaviour can also be assumed. The pit formation on the weld toe in Fig. 5 (b3) suggests that individual pits also initially form along the weld seam line during grooving corrosion and then collapse to form a groove. In addition, the comparison of butt-welded specimens after six and nine months of exposure, Fig. 5 (b3) and (c3), shows that the corroded surface is subject to a large scatter due to its stochastic character and that a clear correlation with the exposure duration is not possible in every case. To address this, a probabilistic investigation of the geometry parameters of the weld seams is required.

3.1.2. *Artificial seawater specimens*

In order to compare the accelerated corrosion in the SSC to the behaviour under seawater conditions, some specimens were stored in ASW for 12 months. Representative results for the fillet-welded specimens are shown in Fig. 6 and for butt-welded specimens in Fig. 7. Similar to the samples in the SSC, deviation and cross-section plots were created.

The fillet welds in Fig. 6 (a3) and (b1) show that the material removal took place both in the HAZ area and in the base material. Compared to the specimens in the SSC, however, the material removal is more uniform and of lower magnitude. This also becomes apparent from the cross-sections lines in Fig. 6 (b2), where the material removal remains almost the same over a length of approx. 10 mm (black line). Despite the differences, however, an increase of the notch radius at the weld toe can be observed due to corrosion, analogous to the specimens in the SSC.

For the butt welds, the removal characteristics are inconsistent. In Fig. 7 (b4) material removal can be observed directly at the weld toe analogous to the SSC specimens, while in Fig. 7 (a4) the area of the weld toe is not affected by material removal at all. This can also be confirmed by the corresponding cross-sections lines in Fig. 7 (c1) and (c2). However, if there is material removal at the weld toe, as shown in Fig. 7 (c2) it leads to grooving corrosion and thus to a sharpening of the notch.

Despite the differences compared to the SSC specimens, the basic behaviour of the weld geometry under corrosive conditions is comparable to that in the SSC. For the fillet welds, the notch is blunted by corrosion, while for the butt welds the notch is sharpened by material removal at the weld toe.

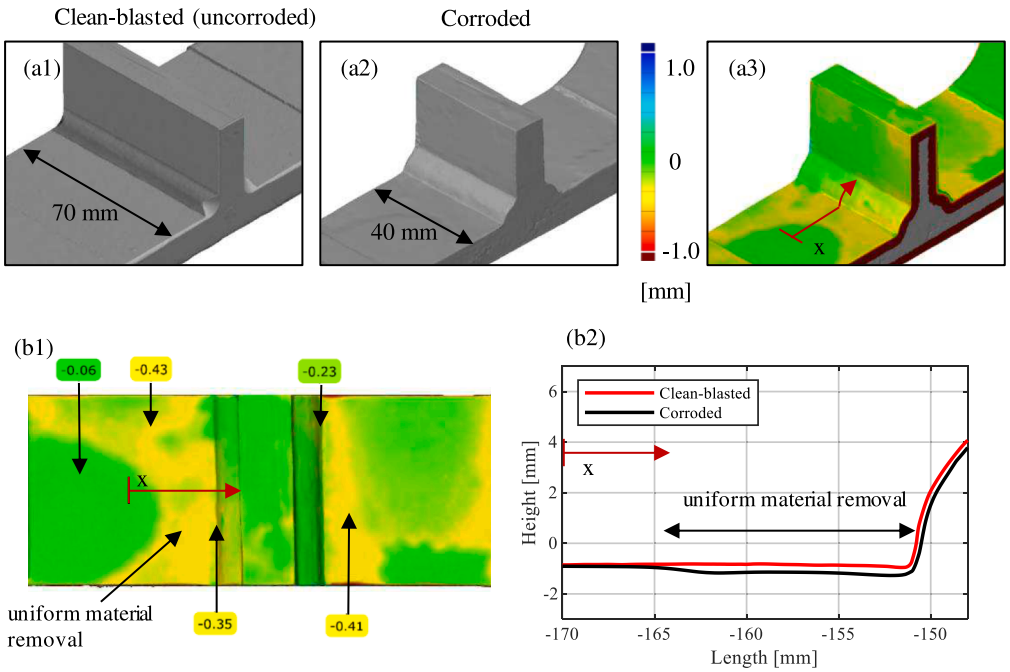

Fig. 6. Representative results of a corroded fillet-welded specimen under corrosive exposure for 12 months in ASW, (a1) scan in uncorroded condition, (a2) scan after corrosion exposure, (a3) deviation plot of the scans, (b1) deviation plot with deviation banners, and (b2) cross section extracted from the scan for the uncorroded and corroded conditions.

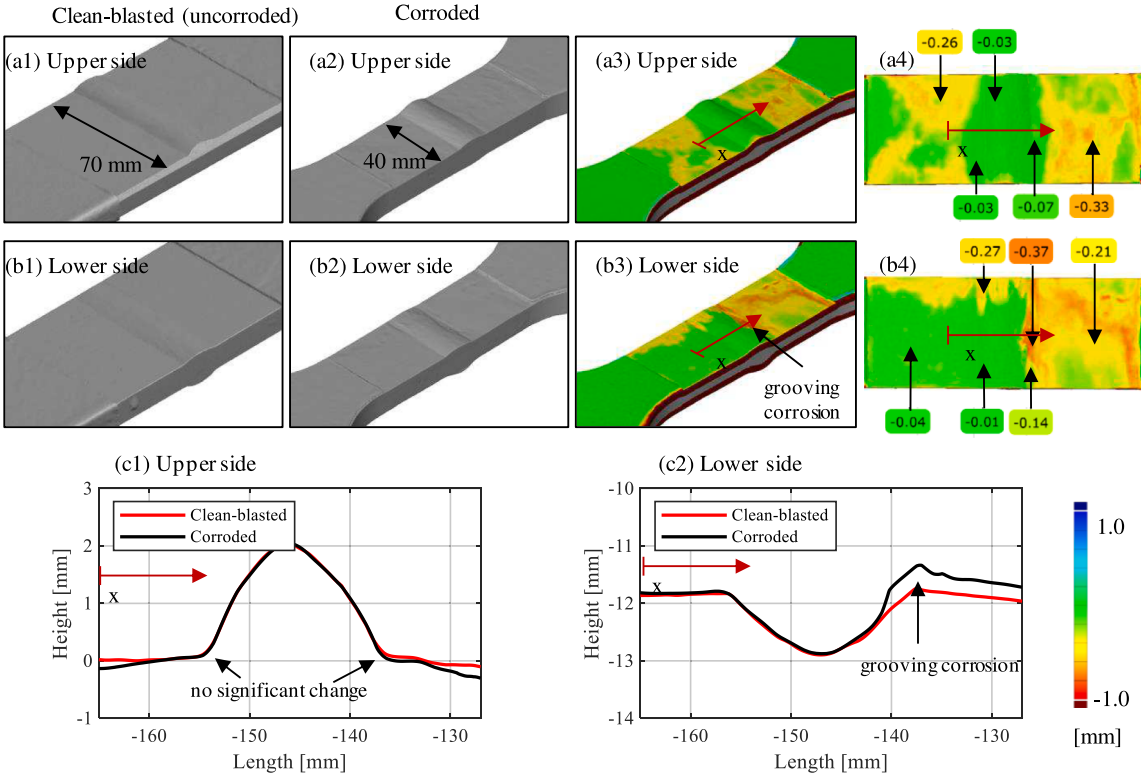

Fig. 7. Representative results of a corroded fillet-welded specimen under corrosive exposure for 12 months in ASW, (a1 and b1) scans in uncorroded condition, (a2 and b2) scans after corrosion exposure, (a3 and b3) deviation plot of the scans, (a4 and b4) deviation plot with deviation banners, and (c1 and c2) cross section extracted from the scan for the uncorroded and corroded conditions.

3.2. Geometrical weld parameter results

The weld seam parameters were determined using the MATLAB script presented in chapter 2.3. For the fillet welds, three specimens with two notch toes each, resulting in six weld toes, were examined for each corrosion duration (3, 6, 9 and 12 months, see chapter 2.1). For the butt welds, only one specimen but including four notch toes were examined for each corrosion duration. Two fillet-welded specimens (3-K-3 and 9-

K-9) were excluded because excessive slag at the weld toe in the AW condition, which would have influenced the scan result and the comparison to the corroded condition.

The scan and the geometrical evaluation results are shown in Fig. 8 and Fig. 9 for fillet and butt welds, respectively. The subplots are organized as follows: The first three rows show the scans of the same specimen in the AW, CB and corroded condition. For each condition, a cross-section through the notch toe at comparable positions for all three surface conditions is plotted in row 4.

However, it is not possible to ensure that the cross-sections in different conditions always have the exact same position, as the entire surface geometry is changed by the corrosion process and there is therefore no reference point. To quantify this influence, additional cross-sections were created at 0.1 to 0.2 mm intervals above and below the main cross-section. The resulting differences were within the resolution of scan of 0.02 mm and can be classified as negligible. Rows 5 and 6 show the probabilistic evaluations of the geometry parameters for the flank angle and the weld toe radius of all cross sections using box plots. The results in the AW, CB, and corroded condition are directly compared. Moreover, row 7 shows SCF calculated according to Anthes' approach comparing all conditions directly with box plots. The columns show the results for different specimens with different corrosion exposure duration, from three to 12 months in the SSC. In addition, the results for radius, flank angle and the SCF with the corresponding mean

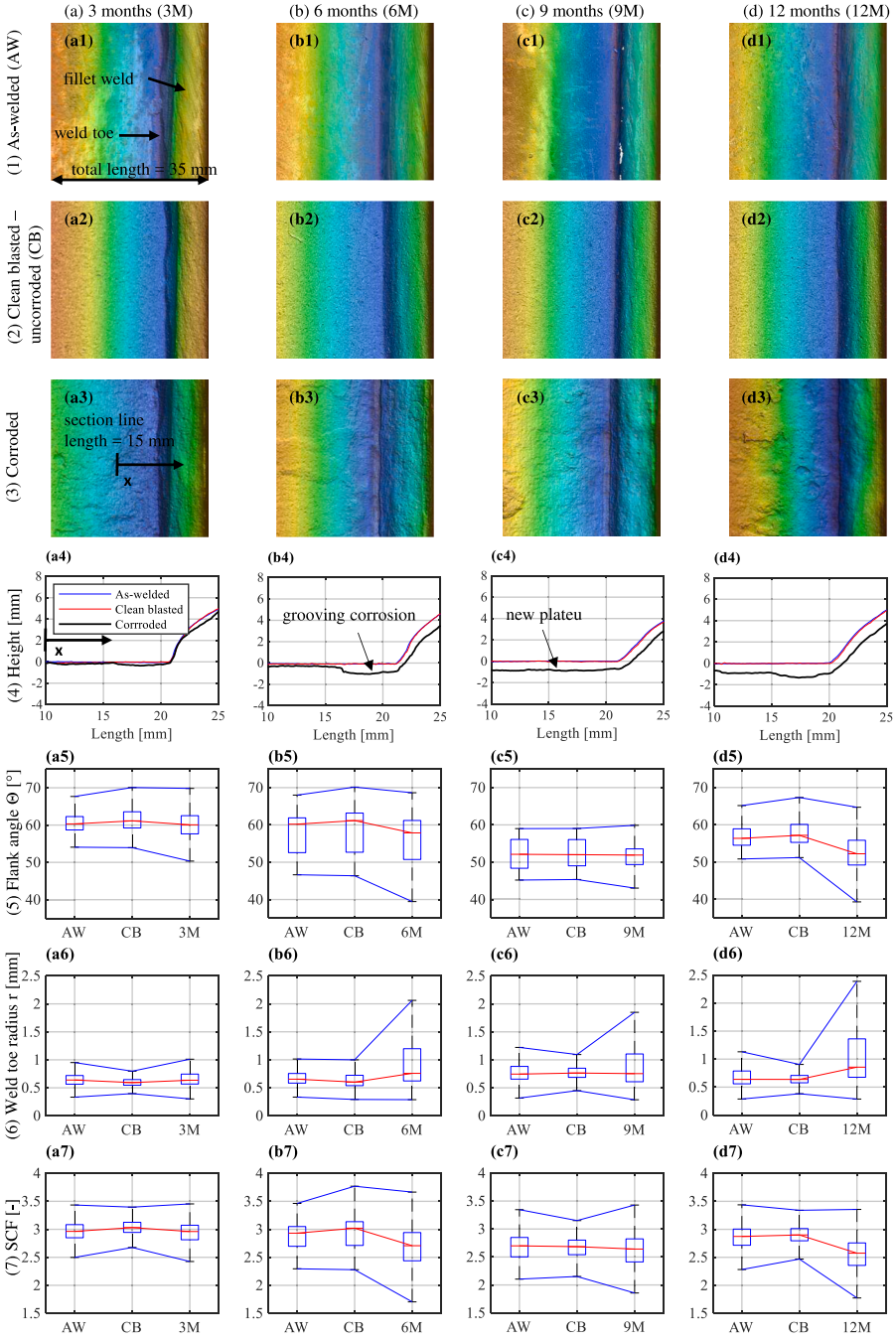

Fig. 8. Results of geometrical change due to corrosion over time for fillet welds, (a1-d1) surface scan in the as-welded condition, (a2-d2) surface scan after clean blasting, (a3-d3) surface scan after corrosion exposure for different time duration, (a4-d4) cross section extracted from the scan for different conditions corrosion durations, (a5-d5) statistical evaluation of the flank angle for different exposure durations, (a6-d6) statistical evaluation of the weld toe radius for different exposure durations, (a7-d7) statistical evaluation of the resulting stress concentrations factor for different exposure durations.

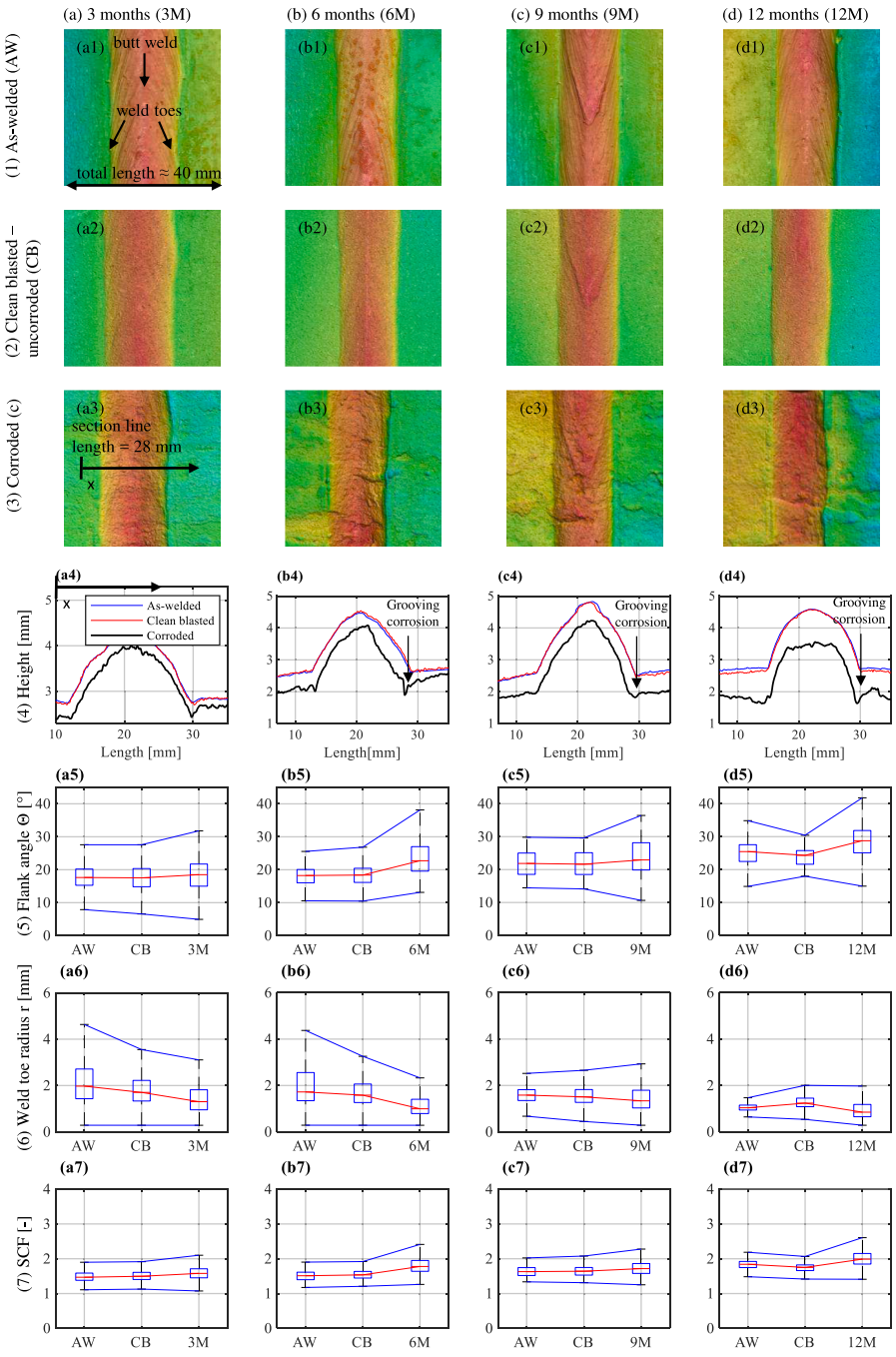

Fig. 9. Results of geometrical change due to corrosion over time for butt welds, (a1-d1) surface scan in the as-welded condition, (a2-d2) surface scan after clean blasting, (a3-d3) surface scan after corrosion exposure for different time duration, (a4-d4) cross section extracted from the scan for different conditions corrosion durations, (a5-d5) statistical evaluation of the flank angle for different exposure durations, (a6-d6) statistical evaluation of the weld toe radius for different exposure durations, (a7-d7) statistical evaluation of the resulting stress concentrations factor for different exposure durations.

values, standard deviations as well as 5 % and 95 % quantile values are presented in Appendix A Table A.1.

3.2.1. *Weld geometry parameters before and after corrosion exposure of SSC specimens*

Results fillet welds (Fig. 8**):** Firstly, it can be concluded from subplots (a4) to (d4) that the profile does not change significantly as a result of clean-blasting. It can be seen that for 3 M and 6 M corroded specimens, there is significant material removal on a length of 5 mm, see subplot (a4) and (b4), near the weld toe in the HAZ. The material removal is part of the grooving corrosion described in chapter 3.1 and is consistent with the results from the digital surface comparisons. This leads the sharp notch at the weld toe to become smoother as the weld toe radius increases and the flank angle decreases. For the 9 M corroded specimen, the base material shows increased uniform corrosion near the weld toe area due to lateral corrosion growth and therefore no groove can be seen. The corroded profile follows the initial AW and CB profile almost parallel, which is at this point the new plateau. As a result, the weld toe radius remains almost the same compared to the initial state. In the 12 M corroded specimens, again grooving corrosion can be seen in an area of 5 mm before the notch toe, but now starting from a new plateau.

The trends of the individual cross-section lines can be confirmed with probabilistic evaluation of the weld parameters shown in subplot (a5) to

(d5) and (a6) to (d6). The geometrical parameters hardly change as a result of clean blasting. The mean value of the flank angle increases in some of the cases (3 M, 6 M, 12 M) and the scattering of the weld toe radius decreases (3 M, 9 M, 12 M), while the mean radius remains unchanged. However, these changes are negligible compared to the changes caused by subsequent corrosion exposure. For the fillet welds, corrosion exposure leads to more significant increase of radius and a decrease in flank angle as well as to a high scattering in both parameters especially for the 6 M and 12 M specimens. However, the 9 M specimens have a change in the scatter of the radius, while the flank angle remains unchanged due to lateral corrosion development.

The stress concentrations in subplots (a7) to (d7) show a higher scattering due to corrosion exposure for all exposure durations. For the 6 M and 12 M specimens the results indicate a significant decrease of the stress concentration, while the 3 M and 9 M specimens show only minor decrease. The extent of the reduction depends on the exposure duration, the cyclical behaviour of the corrosion and on the initial state of the weld geometry. The latter can be observed, for example, in the 9 M specimen, where the stress concentration was initially lower than in the other specimens. This suggests an equalization effect due to corrosion.

Results butt welds (Fig. 9): In contrast to the fillet welds, butt welds show already changes in the weld radius as a result of clean-blasting, while the flank angle does not change, see subplots (a4), (a5) and (a6). Subsequent corrosion exposure leads to a uniform material loss on the weld material and very localized pit/groove formation directly on the weld toe for all exposure duration, see (a4) to (d4). On the one hand, this leads to a greater median flank angle for all exposure durations, see subplot (a5) to (d5), accompanied by a greater scattering. On the other hand, it leads to smaller radii and thus to sharper notches than in the uncorroded state. This can be particularly observed for the 3 M and 6 M specimens in subplots (a6) and (b6), where the median radius decreases from approx. r = 1.7 mm to r = 1.2 mm, accompanied by a decrease in scattering. For the 9 M and 12 M specimens, the radii also decrease, but the scattering increases compared to the initial state. This can be attributed to the observation that, regardless of the initial state, the scattering of the radii is equalized by the corrosion process. In total, both weld geometry parameters lead to an increase of the stress concentrations and their scatter compared to the uncorroded state for all exposure durations, see sub-plot (a7) to (d7). The reason for the contrary behaviour between butt and fillet welds is assumed to lie in different electrochemical potentials, but require further investigation.

Development over time:

In Fig. 10 the geometrical parameters and corresponding stress concentrations for all fillet-welded specimens examined are illustrated over time. The initial conditions (AW and CB) were summarized in a box for all specimens. In addition to the box-plots and the median values, the mean values and the 5 % and 95 % quantile values are presented. For the fillet welds in Fig. 10 a decrease in flank angles and an increase in radii can be observed over time. While the scatter of the flank angles remains the same, the scatter of the radii increases significantly. Overall, this leads to a decreasing stress concentration and a slight increase in scatter over time.

In contrast to the fillet welds, the butt welds in Fig. 11 show an increase of the flank angles and a decrease of the radii over time. While the scatter in the flank angles also remains the same here, the scatter in the radii becomes smaller in contrast to the fillet welds. The resulting stress concentrations grow over time, while the scattering remains approximately the same.

It is evident here that the behaviour of the geometry parameters between fillet and butt welds over time is exactly the opposite. This can be observed, for example, in the 9 M specimens, where the radius of the fillet weld is smaller than the general trend, while the radius of the butt weld is greater than the general trend. It is therefore assumed that the corrosion process results in an equalization effect that causes sharp notches to become smoother, while blunt notches become sharper.

3.2.2. *Weld geometry parameters before and after exposure of ASW specimens*

In Fig. 12 and Fig. 13 the weld geometry parameters for the specimens exposed to ASW are illustrated before and after 12 months corrosive exposure. The fillet welds in Fig. 12 indicate a reduction of the flank angle and an increase of the weld toe radius, which is in line with the results of SSC. The butt welds do not show any clear results due to the inconsistent material removal at the weld toe already described. The flank angle has increased analogously to the SSC. Contrary to expectations, the mean value of the weld toe radius has also increased, while the median value decreased in accordance with the SSC. In total, however, both values lead to a slight increase in the stress concentration, which again corresponds to the behavior under SSC. The quantitative comparison of the mean value before corrosion shows that the stress concentration for this specimen was initially lower compared to the SSC specimens. This is attributed to the circumstance that the specimens for ASW were scanned using the lower resolution scanner GOM ATOS Core 300. This generally leads to insufficient accuracy in reproducing the sharp notches. The comparison between ASW and SSC is further complicated by the fact that only a small number of specimens were examined with the specific exposure time and geometry type. Hence, a quantitative correlation between ASW and SSC is not possible within this investigation.

3.3. *Hardness results*

The hardness measurements were carried out for fillet-welded specimens with varying corrosion exposure durations of 3, 6, 9, and 12 months as well as in the uncorroded (CB) condition as reference. Fig. 14 shows the macrographs and the hardness mappings for all

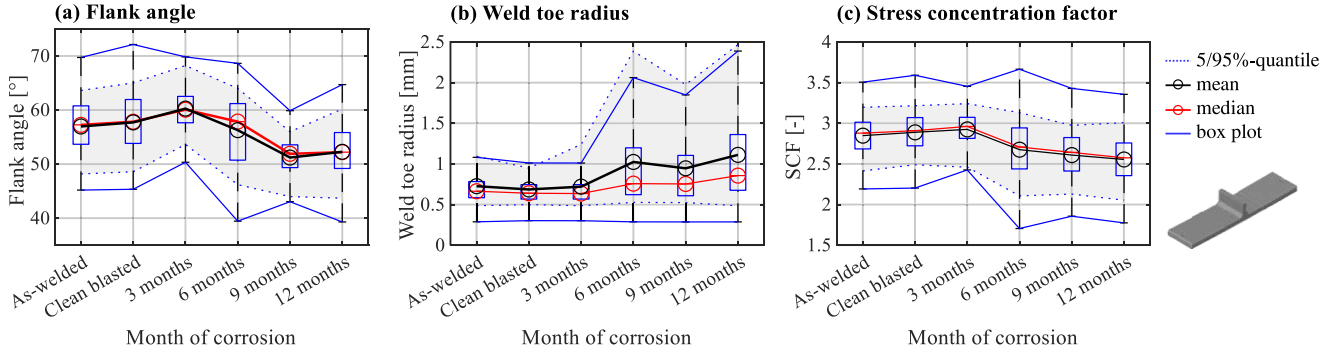

Fig. 10. Development of fillet weld geometry factors: (a) flank angle, (b) weld toe radius, and (c) corresponding stress concentration factors for different exposure durations.

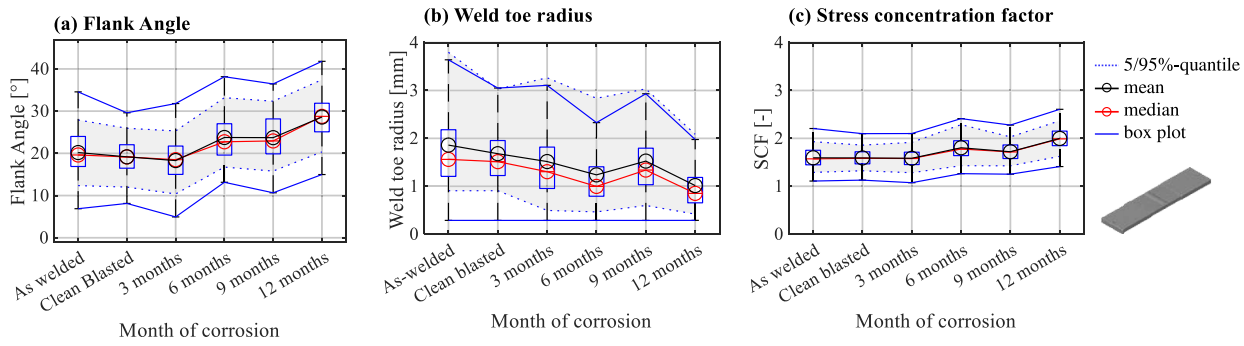

Fig. 11. Development of butt weld geometry factors: (a) flank angle, (b) weld toe radius, and (c) corresponding stress concentration factors for different exposure durations.

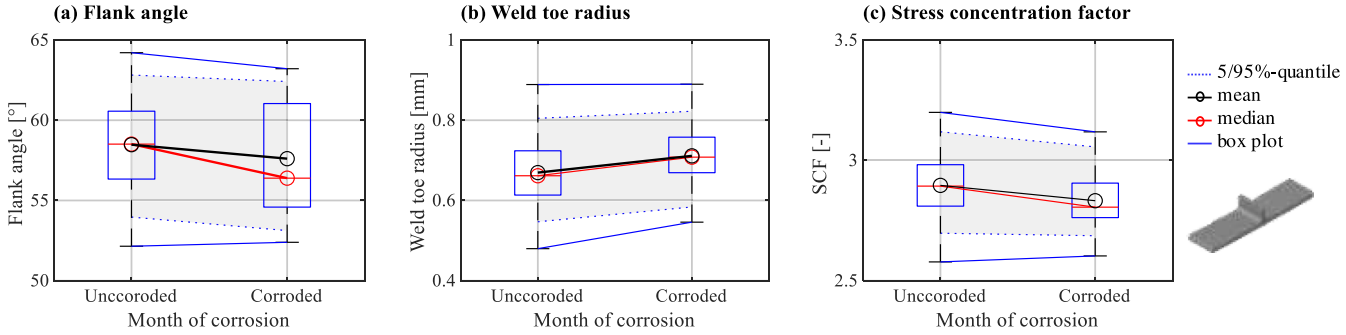

Fig. 12. Statistical evaluation of geometrical parameter before and after corrosion exposure of 12 months in ASW for fillet welds, (a) flank angle, (b) weld toe radius, (c) stress concentrations factor.

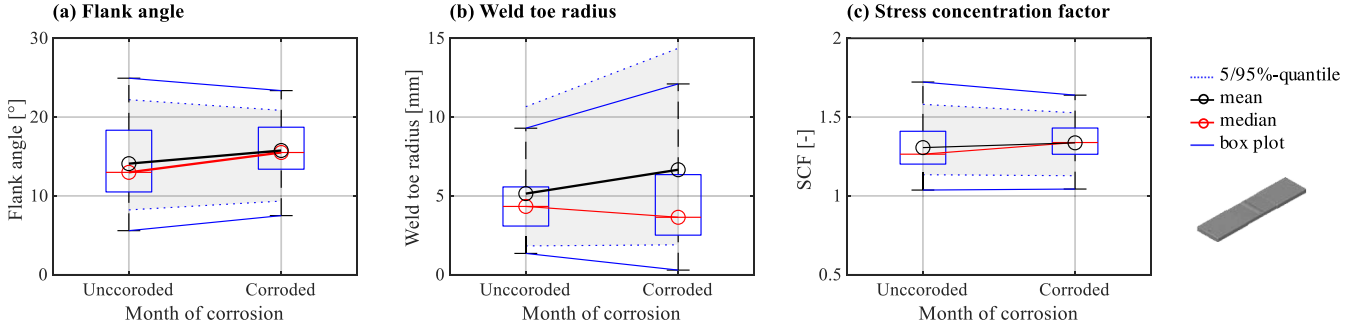

Fig. 13. Statistical evaluation of geometrical parameter before and after corrosion exposure of 12 months in ASW for butt welds, (a) flank angle, (b) weld toe radius, (c) stress concentrations factor.

measured specimens. The differences between the individual zones, weld metal (WM), HAZ and base material (BM) can be seen across all specimens. As expected, the highest hardness values are in the WM and the lowest in the BM. In the HAZ, the values are gradually changing. From the comparison between the uncorroded state in Fig. 14 (d1) and the three-month corroded specimen in Fig. 14 (d2), it can be seen that the hardness values and the distribution have remained almost the same. However, due to the grooving corrosion that took place in the HAZ, the location of the sharpest notch, which in the uncorroded state was on the fusion line between of WM and the HAZ (see subplot (c1)), has shifted to the boundary line of HAZ and BM (see (c2)). Here the overall hardness is lower than at the fusion line between WM and HAZ. The boundary line between HAZ and BM remains as the point of the sharpest notch for both the 6 M and the 9 M (see (c3) and (c4)).

After 12 months, a new notch forms on the newly created plateau, Fig. 14 (c5) and (d5). Although it is less sharp than the notch in the HAZ due to the small opening angle, it is located completely within the BM, where the hardness is lower. The location of the sharper notch shifts from the boundary line of HAZ and BM to the inner part of the HAZ. Thus, the hardness values are higher than in the 3 M to 9 M specimens. However, it can be stated that the hardness values do not change significantly over time due to corrosion, but that the decisive locations of the sharp notches change due to the cyclical progression of corrosion and thus fall into different hardness areas of the specimens.

The 12 M (S) specimens corroded in ASW have higher hardness values in all three areas of the specimens compared to the specimens corroded in SSC, see Fig. 14 (c6) and (d6). In contrast to SSC specimens, the location of the sharpest notch is still at the boundary line of WM and HAZ due to the low material removal, so that no further change in the hardness values results from this.

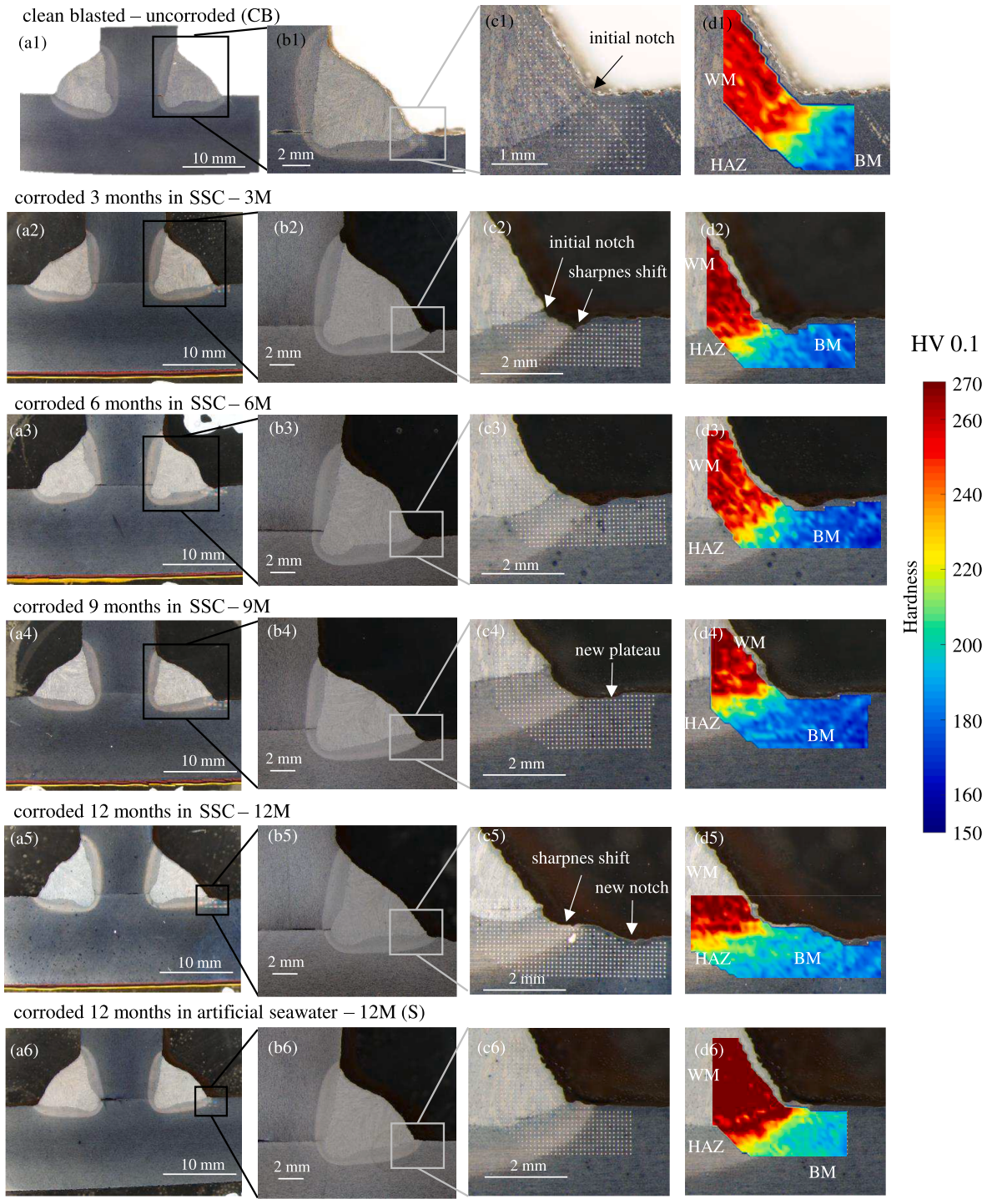

Fig. 14. Micrographs and hardness measurements for uncorroded (a1-d1) and corroded condition for different exposure duration in SSC (a2-d6) as well as for corroded condition after 12-month exposure in ASW (a7-d7).

3.4. Residual stress results

The results of the residual stress measurements are shown in Fig. 15 (a) to (c) for the transversal direction, perpendicular to the weld seam, and in (d) to (f) for the longitudinal direction, parallel to the weld seam. The residual stresses were measured along the paths shown in the figures. The specimens were examined in AW, CB and in several corroded conditions between 1 to 12 months exposure duration. For the AW, CB and 1 M specimens, the measurements were only carried out along one path in the centre of the specimen. For the 3 M, 9 M and 12 M specimens, one measurement was performed in the centre of the specimen, denoted with (1), and one was performed 10 mm to the left, denoted with (2), see Fig. 15 (b). The distance of the measuring points from the weld toe along the paths is shown on the x-axis of the plots. The Y-axis shows the magnitude of the residual stresses, with values above 0 representing tensile residual stresses and below 0 compressive residual stresses.

The highest residual stresses occurred for the transverse stresses directly at the weld toe at the point X = 0 and decrease with increasing distance. For fatigue, the residual stress directly at the weld toe is decisive as this is commonly the critical area of failure. The highest

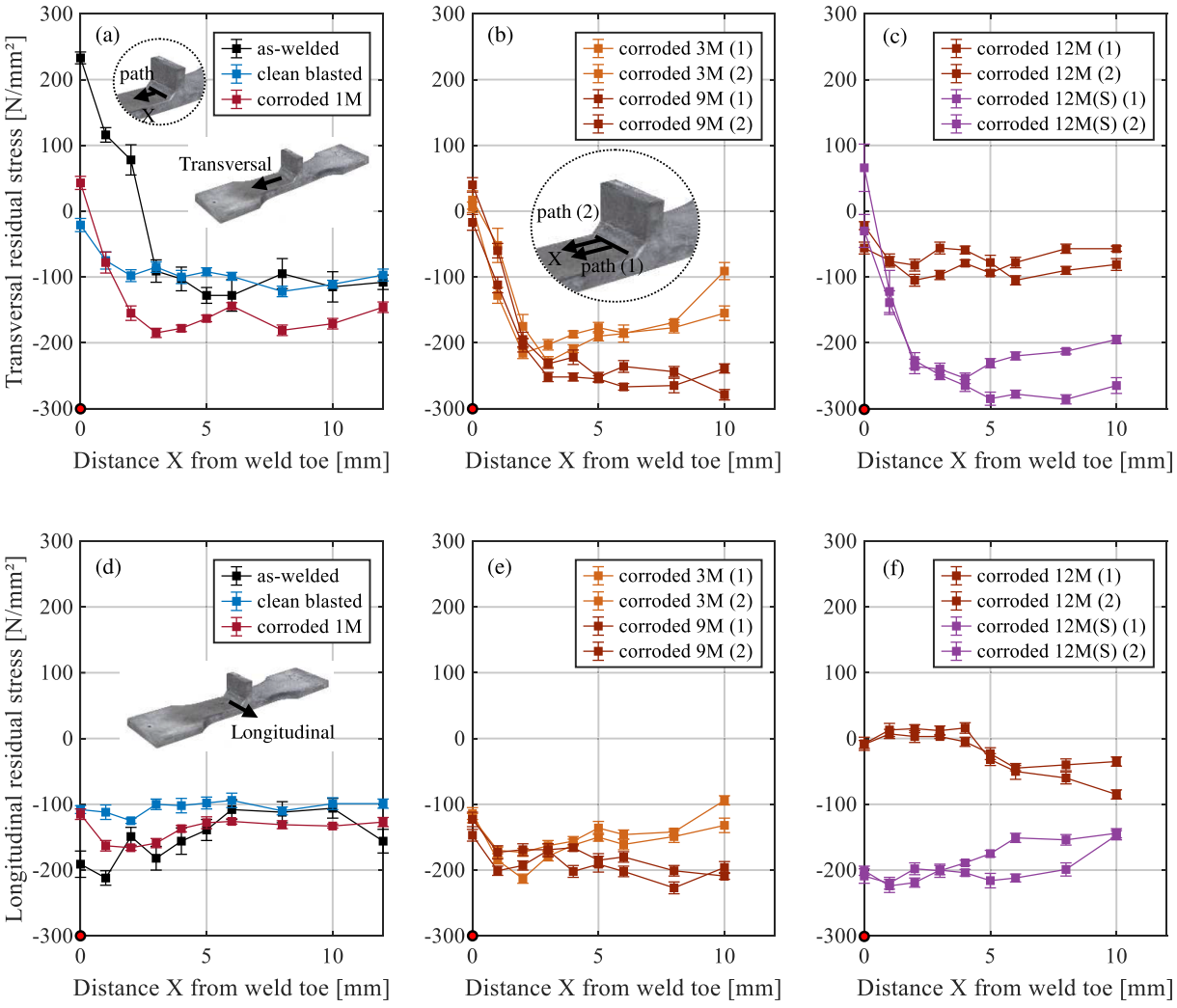

Fig. 15. Residual stress measurements on fillet welds for different corrosion exposure duration, (a)-(c) transversal residual stresses and (d)-(f) longitudinal residual stresses.

residual stress at the weld toe, with over 200 MPa, is found in the AW specimen. The clean blasting generates compressive residual stresses at the surface of the specimen, which leads to the residual stresses falling to $\sigma_{res} \approx 0$ N/mm^2, see Fig. 15 (a). The subsequent corrosion in the 1 M specimen leads to a slight increase in the residual stresses at the weld toe and implies an influence from the corrosion.

However, the measurements in the 3 M, 9 M and 12 M specimen from Fig. 15 (b) and (c) show that the residual stresses at the point $X = 0$ fluctuate around $\sigma_{res} \approx 0$ N/mm^2 despite the progression of corrosion. Fig. 16 shows all measured values of the transverse residual stresses at the point $X = 0$ over the exposure durations. The values show neither a time correlation nor a clear difference between SSC and ASW exposure. The increase in residual stress for the 1 M specimen, which was interpreted as an increase due to corrosion in a previous study [23], lies within the scatter range of all measurements, which here is between -60 N/mm$^2 < \sigma_{res} < 70$ N/mm^2.

Various reasons may explain the scatter in the measured values. Besides the usual factors such as the measuring system or the degree of cleaning of the surface, the redistribution of residual stresses due to local material degradation should be mentioned here, which cannot be quantified without further investigation. This becomes clear from the measurements in the 9 M and 12 M specimen, where a large scatter can be observed on the same specimens (path (1) and path (2)).

On the basis of these findings, it can be assumed that despite existing scattering, the residual stresses do not change significantly after corrosive exposure compared to the initial (clean-blasted) state. This further indicates that the penetration depth of the compressive residual stresses introduced by clean blasting may be higher than the corrosion-induced material removal.

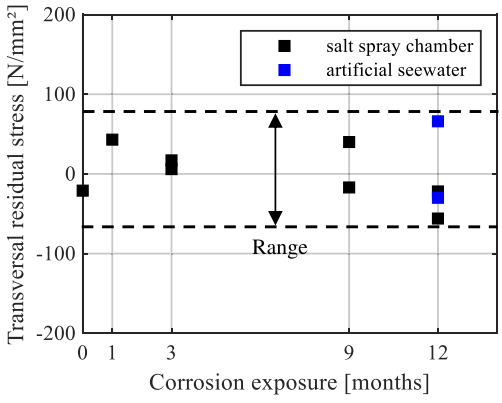

Fig. 16. Development of transversal residual stresses at the weld toe of fillet-welded specimens over corrosion exposure duration.

3.5. Discussion

The results of the geometrical investigations showed clear tendencies despite scattering in the individual values. The notch sharpness, expressed by the SCF, decreased over time in the fillet welds, while it was increased in the butt welds. The reliability of the SCF is influenced not only by the scan resolution but also by the method chosen to determine the SCF. The influence of the scan resolution is considered low for the SSC specimens, due to the high resolution of 0.02 mm. For the ASW specimens, which were scanned with lower resolution of 0.12 mm, the SCF are lower and enable rather qualitative comparisons. The influence of the analytical calculation according to Anthes' formula [14] was investigated by Collmann [47] and resulted in a lower SCF for sharp notches and a higher SCF for weak notches compared to the numerical calculation. As the SCF was used for comparative purposes in this study, the inaccuracy of the analytical formula is tolerated. For investigations of the fatigue strength of corroded components, it is recommended to use a numerical calculation based on the weld geometry data provided in Appendix A. However, the geometrical parameter results are consistent with the results of Matsushita et al. [16], who observed grooving corrosion in the HAZ for both fillet and butt welds. Furthermore, the findings of Yuasa and Watanabe [17], who observed a greater reduction in fatigue strength in butt welds than in fillet welds, can be explained. At this point, it's relevant to point out that the results are based on limited specimens, especially for butt welded joints. Due to the stochastic nature of corrosion, it is important to increase the number of experiments in future studies for greater statistical significance of the findings.

Hardness measurements around the weld toe showed minor changes due to corrosion, but the sharpest, fatigue-relevant notch shifted over time from the fusion line (WM/HAZ boundary) to the HAZ/BM boundary. This spatial shift implies a change in fatigue-relevant hardness, as the WM has the highest hardness and the BM the lowest. This can lead to insufficient results when attempting to predict the fatigue strength, as it is usually assumed that the high stress concentrations at the weld toe are also the location of the lowest material quality in fatigue strength analysis.

Residual stress analysis revealed no clear correlation with corrosion duration, with the initial state only marginally affected despite potential internal redistribution from material removal. It is assumed that the penetration depth of the compressive residual stresses introduced by clean blasting may be higher than the corrosion-induced material removal. This should be investigated in future studies using the hole drilling method to determine the residual stress in the thickness direction. In addition, the number of experiments should be increased in future studies in order to increase the significance of the results.

It should be noted that the hardness and residual stress measurements were carried out on different specimen for each point in time and therefore the development over time does not represent the actual development of an individual specimen. For this, the specimen would have to be further corroded again after the residual stress measurements, which would result in multiple corrosion and rust removal processes that does not correspond to reality because it influences the corrosion behaviour. Nevertheless, the measurements provide initial insights into the long-term behaviour due to the low scattering of the results.

It is important to highlight, that the specimens investigated in this study were subjected either to corrosion under SSC or ASW, which do not reflect the real offshore environment. A transfer to real offshore structures is therefore not directly possible. However, in view of the fact that corresponding fatigue tests from the literature also do not reflect the real environmental conditions, the findings of this study can be at least used as an explanation for the different fatigue test results of butt and fillet welds in the literature.

4. Summary and conclusion

The aim of this study has been to quantify the influence of corrosion on the fatigue-driving parameters such as notch stress concentration, local hardness conditions and residual stresses over time. The focus was on the long-term development, which aimed to be achieved by accelerated corrosion in the salt spray chamber over a total period of 12 months. Both butt-welded and fillet-welded specimens were examined.

To determine the notch stress concentration and its change over time, the specimens were recorded before and after corrosive exposure and evaluated with regard to the decisive weld geometry parameters. Subsequent hardness and residual stress measurements were carried out on the fillet-welded joints.

The following findings can be drawn from this study.

- **Digital surface comparison:** It has been shown that pitting corrosion can occur directly on the fatigue-relevant area of the weld toe in both butt and fillet welds. As the exposure duration progresses, further pits develop along the weld toe line, which then form grooves parallel to the weld seam. With corrosion progression, the material next to the resulting grooves is also degraded, leading to a new plateau (uniform corrosion). On the new plateau, the process described from pitting to grooving and then to new plateau is repeated.
- **Weld geometry analysis**: By investigating the geometrical parameters, it was possible to show that welded components behave differently depending on the initial notch sharpness with regard to corrosive effects. It could be quantitatively shown that the notch radius for butt welds, has decreased over time, while an increase has taken place for fillet welds. Similarly, the flank angle increased for butt welds, while it decreased for fillet welds. This leads to the conclusion that corrosive impact on butt welds, which have shallow notches compared to fillet welds, leads to an increase in notch sharpness, while the sharp notches of the fillet welds become shallower over time. This behaviour can be described as an equalization effect of corrosion.
- **Hardness measurements**: The hardness measurements, which concentrated on the weld toe area, showed only minor changes due to corrosion. However, it was observed that the location of the sharpest and therefore fatigue-relevant notch varied over time. While the sharpest notch before corrosion was located between the fusion line of the weld metal (WM) and the heat affected zone (HAZ), it moved over time to the boundary line between the HAZ and the base material (BM). In consideration of the fact that the highest hardness values are present in the WM and the lowest in the BM, a changing fatigue-relevant hardness can be assumed due to the spatial change of the sharpest notch.
- **Residual stress analysis**: The residual stress measurements have shown that there is no clear correlation with corrosion exposure duration and that the initial state is only marginally affected, despite possible internal redistribution from material removal.

The presented results allow new insight into the long-term behaviour of corrosion on the fatigue-relevant parameters. In addition, the obtained results provide a basis for future investigations of the (residual) service life of corroded load-bearing structures using local fatigue approaches such as the notch stress concept according to IIW or the 4R method. The calculations can be carried out either deterministically with the mean values or probabilistically using the data of the geometrical parameters provided in this study.

CRediT authorship contribution statement

Sulaiman Shojai: Writing – original draft, Visualization, Validation, Supervision, Resources, Project administration, Methodology, Investigation, Funding acquisition, Formal analysis, Data curation, Conceptualization. **Finn Schönamsgruber:** Writing – original draft, Visualization, Investigation, Formal analysis. **Markus Köhler:** Writing – review & editing, Resources, Investigation. **Elyas Ghafoori:** Writing –

review & editing, Supervision, Project administration.

Declaration of competing interest

The authors declare that they have no known competing financial interests or personal relationships that could have appeared to influence the work reported in this paper.

Acknowledgements

The research project "Influence of corrosive media on the fatigue strength of offshore wind turbines (CorroFAT)", grant number 37 LN/1, of the Research Association for Steel Applications (FOSTA) e. V. was funded by the German Federal Ministry of Economics and Climate Action (BMWK) via the German Federation of Industrial Research Associations "Otto von Guericke" (AiF) e. V. as part of the program "Leittechnologien für die Energiewende" and as part of the joint project "Offshore Wind Energy Systems for Hydrogen Supply" to promote joint industrial research (IGF) on the basis of a resolution of the German Bundestag. The authors would like to express their sincere gratitude for the experienced financial support.

Appendix A. Weld geometry data of investigated specimens in different conditions

Table A1
Probabilistic data for weld toe radius r, flank angle θ, and the resulting SCF for fillet- and butt welded specimens with different exposure duration.

	Fillet welds Radius r [mm]						Butt welds Radius r [mm]					
	AW	CB	3 M	6 M	9 M	12 M	AW	CB	3 M	6 M	9 M	12 M
Mean E	0.73	0.69	0.72	1.02	0.95	1.11	1.86	1.68	1.52	1.24	1.53	1.01
Std. Dev.	0.32	0.25	0.34	0.64	0.51	0.68	1.05	0.72	0.91	0.78	0.82	0.59
5 %-quantile	0.49	0.50	0.49	0.53	0.52	0.48	0.91	0.91	0.50	0.46	0.60	0.42
95 %-quantile	1.09	0.95	1.24	2.39	1.98	2.47	3.80	3.03	3.27	2.84	3.03	2.09
	Flank angle θ [°]						**Flank angle θ [°]**					
	AW	**CB**	**3 M**	**6 M**	**9 M**	**12 M**	**AW**	**CB**	**3 M**	**6 M**	**9 M**	**12 M**
Mean E	57.0	57.7	60.3	56.3	51.2	52.3	20.2	19.2	18.3	23.8	23.7	28.6
Std. Dev.	4.8	5.2	4.0	6.0	3.4	4.9	4.9	4.1	4.7	5.4	5.3	5.2
5 %-quantile	18.2	48.6	53.6	46.2	44.0	43.7	12.4	12.0	10.4	16.7	15.8	20.3
95 %-quantile	63.6	65.0	68.2	64.0	56.0	60.2	27.9	25.9	25.3	33.2	32.3	37.4
	SCF [-]						**SCF [-]**					
	AW	**CB**	**3 M**	**6 M**	**9 M**	**12 M**	**AW**	**CB**	**3 M**	**6 M**	**9 M**	**12 M**
Mean E	2.85	2.89	2.92	2.68	2.61	2.55	1.59	1.59	1.58	1.80	1.72	2.00
Std. Dev.	0.25	0.24	0.24	0.32	0.27	0.30	0.20	0.17	0.21	0.25	0.22	0.24
5 %-quantile	2.41	2.49	2.46	2.11	2.13	2.05	1.29	1.32	1.28	1.43	1.43	1.62
95 %-quantile	3.20	3.22	3.24	3.13	2.97	3.01	1.93	1.86	1.92	2.29	2.03	2.37

During the preparation of this work the authors used ChatGPT and DeepL in order to improve the language. After using these tools, the authors reviewed and edited the content as needed and take full responsibility for the content of the publication.

Appendix B. Supplementary data

Supplementary data to this article can be found online at https://doi.org/10.1016/j.matdes.2024.113578.

Data availability

No data was used for the research described in the article.

References

[1] L. Xiang, J. Pan, S. Chen, Analysis on the stress corrosion crack inception based on pit shape and size of the FV520B tensile specimen, Results Phys. 9 (2018) 463–470, https://doi.org/10.1016/j.rinp.2018.03.005.
[2] M. Cerit, Corrosion pit-induced stress concentration in spherical pressure vessel, Thin-Walled Struct. 136 (2019) 106–112, https://doi.org/10.1016/j.tws.2018.12.014.
[3] Y. Huang, C. Wei, L. Chen, P. Li, Quantitative correlation between geometric parameters and stress concentration of corrosion pits, Eng. Fail. Anal. 44 (2014) 168–178, https://doi.org/10.1016/j.engfailanal.2014.05.020.
[4] X. Liang, J. Sheng, K. Wang, Investigation of the mechanical properties of steel plates with artificial pitting and the effects of mutual pitting on the stress concentration factor, Results Phys. 14 (2019) 102520, https://doi.org/10.1016/j.rinp.2019.102520.
[5] J. Hou, L. Song, Numerical Investigation on Stress Concentration of Tension Steel Bars with One or Two Corrosion Pits, Adv. Mater. Sci. Eng. 2015 (2015) 1–7, https://doi.org/10.1155/2015/413737.
[6] S. Shojai, P. Schaumann, T. Brömer, Probabilistic modelling of pitting corrosion and its impact on stress concentrations in steel structures in the offshore wind energy, Mar. Struct. 84 (2022) 103232, https://doi.org/10.1016/j.marstruc.2022.103232.
[7] Anthes RJ, Köttgen VB, SEEGER T. Einfluss der Nahtgeometrie auf die Dauerfestigkeit von Stumpf-und Doppel-T-Stossen; 1994.
[8] B. Schork, P. Kucharczyk, M. Madia, U. Zerbst, J. Hensel, J. Bernhard, et al., The effect of the local and global weld geometry as well as material defects on crack initiation and fatigue strength, Eng. Fract. Mech. 198 (2018) 103–122, https://doi.org/10.1016/j.engfracmech.2017.07.001.
[9] B. Schork, U. Zerbst, Y. Kiyak, M. Kaffenberger, M. Madia, M. Oechsner, Effect of the parameters of weld toe geometry on the FAT class as obtained by means of fracture mechanics-based simulations, Weld World 64 (6) (2020) 925–936, https://doi.org/10.1007/s40194-020-00874-7.
[10] G. Hultgren, Z. Barsoum, Fatigue assessment in welded joints based on geometrical variations measured by laser scanning, Weld World 64 (11) (2020) 1825–1831, https://doi.org/10.1007/s40194-020-00962-8.
[11] Z. Barsoum, B. Jonsson, Influence of weld quality on the fatigue strength in seam welds, Eng. Fail. Anal. 18 (3) (2011) 971–979, https://doi.org/10.1016/j.engfailanal.2010.12.001.
[12] International Standards Organization. ISO 5817: Welding – Fusion-welded joints in steel, nickel, titanium and their alloys (beam welding excluded) – Quality levels for imperfections; 2014.

[13] F.V. Lawrence, N.J. Ho, P.K. Mazumdar, Predicting the Fatigue Resistance of Welds, Annu. Rev. Mater. Sci. 11 (1) (1981) 401–425, https://doi.org/10.1146/annurev.ms.11.080181.002153.
[14] Anthes RJ, Köttgen VB, SEEGER T. Kerbformzahlen von Stumpfstößen und Doppel-T-Stößen. Schweißen und Schneiden 1993(45 (12)):685–8.
[15] Y. Kiyak, M. Madia, U. Zerbst, Extended parametric equations for weld toe stress concentration factors and through-thickness stress distributions in butt-welded plates subject to tensile and bending loading, Weld World 60 (6) (2016) 1247–1259, https://doi.org/10.1007/s40194-016-0377-x.
[16] H. Matsushita, T. Nakai, N. Yamamoto, A Study on Static Strength of Corroded Fillet Welded Joints for Ship Structures, Journal of the Society of Naval Architects of Japan (2004).
[17] M. Yuasa, T. Watanabe, Fatigue Strength of Corroded Weld Joints, ClassNK Technical Bulletin 14 (1996) 51–61.
[18] M. Jakubowski, Influence of pitting corrosion on fatigue and corrosion fatigue of ship structures Part I Pitting corrosion of ship structures, Pol. Marit. Res. 21 (1) (2013) 62–69, https://doi.org/10.2478/pomr-2014-0009.
[19] ASTM International. Standard Practice for Preparation of Substitute Ocean Water (ASTM D1141); 1998.
[20] International Standards Organization, ISO 9227: Corrosion tests in artificial atmospheres – Salt spray tests, Beuth, Berlin, 2017.
[21] S. Gkatzogiannis, J. Weinert, I. Engelhardt, P. Knoedel, T. Ummenhofer, Correlation of laboratory and real marine corrosion for the investigation of corrosion fatigue behaviour of steel components, Int. J. Fatigue 126 (2019) 90–102, https://doi.org/10.1016/j.ijfatigue.2019.04.041.
[22] J. Weinert, S. Gkatzogiannis, I. Engelhardt, P. Knoedel, T. Ummenhofer, Investigation of corrosive influence on the fatigue behaviour of HFMI-treated and as-welded transverse non-load-carrying attachments made of mild steel S355, Int. J. Fatigue 151 (2021) 106225, https://doi.org/10.1016/j.ijfatigue.2021.106225.
[23] S. Shojai, T. Brömer, E. Ghafoori, C. Woitzik, M. Braun, M. Köhler, et al., Assessment of corrosion fatigue in welded joints using 3D surface scans, digital image correlation, hardness measurements, and residual stress analysis, Int. J. Fatigue 176 (2023) 107866, https://doi.org/10.1016/j.ijfatigue.2023.107866.
[24] J. Baumgartner, T. Bruder, Influence of weld geometry and residual stresses on the fatigue strength of longitudinal stiffeners, Weld World 57 (6) (2013) 841–855, https://doi.org/10.1007/s40194-013-0078-7.
[25] J. Krebs, M. Kassner, Influence of Welding Residual Stresses on Fatigue Design of Welded Joints and Components, Weld World 51 (7–8) (2007) 54–68, https://doi.org/10.1007/BF03266586.
[26] H.R. Raftar, A. Ahola, K. Lipiäinen, T. Björk, Simulation and experiment on residual stress and deflection of cruciform welded joints, J. Constr. Steel Res. 208 (2023) 108023, https://doi.org/10.1016/j.jcsr.2023.108023.
[27] S. Shojai, T. Brömer, E. Ghafoori, P. Schaumann, Application of local fatigue approaches on corroded welded joints with consideration of weld geometry and residual stresses, Theor. Appl. Fract. Mech. (2023) 104215, https://doi.org/10.1016/j.tafmec.2023.104215.
[28] J. Hensel, T. Nitschke-Pagel, D. Tchoffo Ngoula, H.-T. Beier, D. Tchuindjang, U. Zerbst, Welding residual stresses as needed for the prediction of fatigue crack propagation and fatigue strength, Eng. Fract. Mech. 198 (2018) 123–141, https://doi.org/10.1016/j.engfracmech.2017.10.024.
[29] M. Braun, J. Hensel, S. Song, S. Ehlers, Fatigue strength of normal and high strength steel joints improved by weld profiling, Engineering Archive (2021).
[30] A. Ahola, A. Muikku, M. Braun, T. Björk, Fatigue strength assessment of ground fillet-welded joints using 4R method, Int. J. Fatigue 142 (2021) 105916, https://doi.org/10.1016/j.ijfatigue.2020.105916.
[31] T. Nykänen and T. Björk. A new proposal for assessment of the fatigue strength of steel butt-welded joints improved by peening (HFMI) under constant amplitude tensile loading.
[32] T. Pesonen, J. Riski, K. Lipiäinen, A. Ahola, T. Björk, Framework for a finite element method-based simulation approach to fatigue assessment of welded joints using the 4R method, Int. J. Fatigue (2024) 108148, https://doi.org/10.1016/j.ijfatigue.2024.108148.
[33] A. Ahola, K. Lipiäinen, S. Afkhami, H. Lilja, T. Björk, Fatigue performance of the welded details of an old, demolished steel railway bridge, Eng. Struct. 256 (2022) 113966, https://doi.org/10.1016/j.engstruct.2022.113966.
[34] International Standards Organization. ISO 8501-1:2007-12; Preparation of steel substrates before application of paints and related products - Visual assessment of surface cleanliness - Part 1: Rust grades and preparation grades of uncoated steel substrates and of steel substrates after overall removal of previous coatings (ISO 8501-1:2007).
[35] Det Norske Veritas. Corrosion protection for wind turbines(DNV-GL RP-0416); 2016.
[36] Iso, 8407: Corrosion of metals and alloys – Removal of corrosion products from corrosion test specimens, Beuth, Berlin, 2021.
[37] D. Taylor, The theory of critical distances, Eng. Fract. Mech. 75 (7) (2008) 1696–1705, https://doi.org/10.1016/j.engfracmech.2007.04.007.
[38] F. Renken, Bock und Polach RUF von, J. Schubnell, M. Jung, M. Oswald, K. Rother, et al., An algorithm for statistical evaluation of weld toe geometries using laser triangulation, Int. J. Fatigue 149 (2021) 106293, https://doi.org/10.1016/j.ijfatigue.2021.106293.
[39] J. Schubnell, M. Jung, C. Hieu Le, F. Majid, M. Braun, S. Ehlers, et al., Influence of the optical measurement technique and evaluation approach on the determination of local weld geometry parameters for different weld types, Weld World 64 (2) (2020) 301–316, https://doi.org/10.1007/s40194-019-00830-0.
[40] C. Dänekas, S. Heikebrügge, J. Schubnell, P. Schaumann, B. Breidenstein, B. Bergmann, Influence of deep rolling on surface layer condition and fatigue life of steel welded joints, Int. J. Fatigue 162 (2022) 106994, https://doi.org/10.1016/j.ijfatigue.2022.106994.
[41] C. Dänekas, P. Schaumann, E. Ghafoori, S. Heikebrügge, K.M. Heide, B. Breidenstein, Development of an automated quality assurance approach for welded joints, Ce Papers 6 (3–4) (2023) 2510–2515, https://doi.org/10.1002/cepa.2439.
[42] K.M. Heide, S. Heikebrügge, C. Dänekas, B. Breidenstein, P. Schaumann, Automated geometry measurement and deep rolling of butt welds, Weld World 66 (12) (2022) 2533–2547, https://doi.org/10.1007/s40194-022-01346-w.
[43] International Standards Organization. ISO 6507-1, Metallic materials — Vickers hardness test — Part 1: Test method;2022.
[44] R.E. Melchers, Progress in developing realistic corrosion models, Struct. Infrastruct. Eng. 14 (7) (2018) 843–853, https://doi.org/10.1080/15732479.2018.1436570.
[45] C. Kato, Y. Otoguro, S. Kado, Y. Hisamatsu. Grooving corrosion in electric resistance welded steel pipe in sea water. Corrosion Science 1978;1978(Vol. 18): 61–74.
[46] P.D. Bilmes, C.L. Llorente, C.M. Méndez, C.A. Gervasi, Microstructure, heat treatment and pitting corrosion of 13CrNiMo plate and weld metals, Corros. Sci. 51 (4) (2009) 876–881, https://doi.org/10.1016/j.corsci.2009.01.018.
[47] M. Collmann, Ermüdungsfestigkeit von Stumpfnahtverbindungen größerer Blechdicke gefügt mit Hochleistungsschweißverfahren, Hannover Institutionelles Repositorium Der Leibniz Universität Hannover (2021).